Polymer 50 (2009) 2081–2086

Contents lists available at ScienceDirect

Polymer

journal homepage: www.elsevier.com/locate/polymer

Microporous membranes prepared via thermally induced phase separation from metallocenic syndiotactic polypropylenes

Ma. Eulalia Vanegas [a,*], Raúl Quijada [a], Daniel Serafini [b]

[a] Departamento de Ingeniería Química y Biotecnología, Facultad de Ciencias Físicas y Matemáticas, Universidad de Chile, and Centro para la Investigación Interdisciplinaria Avanzada en Ciencias de los Materiales (CIMAT), Casilla 2777, Santiago, Chile
[b] Departamento de Física, Facultad de Ciencia, Universidad de Santiago de Chile, Casilla 10233, Santiago, Chile

ARTICLE INFO

Article history:
Received 19 November 2008
Received in revised form
3 March 2009
Accepted 7 March 2009
Available online 18 March 2009

Keywords:
Syndiotactic polypropylene
Microporous membranes
TIPS process

ABSTRACT

Microporous membranes were prepared by thermally induced phase separation (TIPS) using different tailor-made syndiotactic polypropylenes (sPP) synthesized by metallocene catalysts. The phase diagrams of sPP samples in diphenyl ether (DPE) were determined. The polymer microstructure effect on the thermodynamic and kinetic properties of the sPP–DPE systems were also determined and correlated with membrane pore size. The crystal structure which developed in the matrix of the porous membranes was investigated by wide-angle X-ray diffraction (WXRD). The cloud points were found to be slightly affected by molecular weight (M_w) and the influence of syndiotacticy was negligible. The dynamic crystallization curves depended solely on the syndiotacticity of the samples, shifting to lower temperatures as the stereoregularity of the sPP decreased, and no relation with M_w was found. The viscosity of sPP–DPE solutions increased with M_w and stereoregularity of the sPP. Membrane pore sizes were correlated with droplet growth period, crystallization behaviour, and sample viscosity, the latter being an important parameter for low polymer solution concentration (15 wt%) but not so at higher concentration (40 wt%). The results showed that by controlling polymer microstructure it is possible to control membrane pore size.

1. Introduction

Polymer membranes have rapidly gained substantial importance in chemical technology and are used in a large number of practical applications [1]. Membrane preparation techniques are important for controlling the properties of membrane materials. The ability to control pore size is desirable for membrane manufacturers because this property is important for performance characteristics [2]. In this context, the thermally induced phase separation (TIPS) process introduced by Castro [3] is one of the most important techniques for the preparation of microporous polymer membranes by controlled phase separation [4]. Compared to non-solvent induced phase separation (NIPS), the main advantage of the TIPS process is that it makes it easier to control membrane structure because there are fewer factors influencing porous structure [5,6]. In general, polymer microporous membranes are used for a wide variety of industrial applications covering the entire ultra- and microfiltration range [7]. New applications for these membranes such as separators in rechargeable batteries [6,8] or as supports for manufacturing thin film composite membranes for nanofiltration by interfacial polymerization have also been reported [9].

The TIPS process involves heating a polymer in a diluent to a sufficiently high temperature for melt-blending the components into a homogenous phase. The diluent is usually a low molecular weight, high-boiling point solvent in which the polymer is not soluble at room temperature, but solubilizes the polymer at higher temperatures. When the homogenous solution is cooled, phase separation is induced. Through the appropriate choice of diluent and initial polymer concentration, cooling the solution leads to a liquid–liquid phase separation to form two phases consisting of a diluent-rich droplets phase surrounded by a polymer-rich liquid matrix phase. Upon further cooling, the matrix phase solidifies and locks in the droplets within the solid matrix and subsequently the diluent is extracted [10].

A number of different semicrystalline polymers, especially isotactic polypropylenes (iPP) are widely used in the TIPS process. TIPS mechanisms and the influence of initial polymer solution composition, cooling rate, nucleating agent addition, and droplet growth kinetics on membrane morphology were investigated by Lloyd et al. [11–13]. On the other hand, the effect of iPP molecular

* Corresponding author. Tel.: +56 2 9784188; fax: +56 2 6991084.
E-mail address: evanegas@ciq.uchile.cl (Ma.E. Vanegas).

0032-3861/$ – see front matter © 2009 Elsevier Ltd. All rights reserved.
doi:10.1016/j.polymer.2009.03.006

weight and kind of diluent on microporous morphology and the use of polymer blends in the preparation of porous membranes were reported by Matsuyama et al. [14–16]. Different types of polypropylenes and of iPP-1-hexene copolymers were also investigated in order to study the formation of porous membranes [17,18]. The effect of the mixed diluent composition on membrane morphology and iPP crystallization behavior has also been reported [19]. Most of these studies were focused on the highly successful commercial isotactic form of polypropylene. The results showed that membranes with different porous structures (inter-connected or cellular pores) can be fabricated depending on polymer solution properties and preparation conditions. However, new metallocene catalysts have been developed which are capable of producing highly stereo and regioregular syndiotactic polypropylene (sPP) under well controlled conditions [20]. sPP has properties different from those of iPP, such as higher viscosity, greater flexibility, different crystalline forms [21,22], and greater resistance to oxidative degradation, making it an attractive material for polymer membrane applications. Previously we have reported on the synthesis and investigation of one sPP sample for membrane preparation and its final morphology by the TIPS process [23,24], but a larger study focused on sPP samples with different microstructure must be researched further.

In this work the effect of syndiotacticity and molecular weight of sPP samples on polymer–diphenyl ether phase diagrams and viscosity were studied. The TIPS process was used to prepare microporous sPP membranes. The effect of the different polymer microstructures on crystallinity and final membrane structure, especially pore morphology, were studied.

2. Experimental part

2.1. Materials

All polypropylenes were synthesized with the syndioselective metallocene catalysts $(Me)_2C(Cp)(9\text{-}Flu)ZrCl_2$ (Cat A) and $Ph_2C(Cp)(9\text{-}Flu)ZrCl_2$ (Cat B) from Boulder Scientific, with methylaluminoxane (MAO) as cocatalyst from Aldrich (10% w/v in toluene). Solvent toluene was distilled over sodium in an inert atmosphere. Propene, from Petroquim S.A., was deoxygenated and dehydrated by passing through columns containing Cu catalysts (BASF, R3-11G and R3-12), and 4 Å molecular sieves, respectively.

For membrane preparation, diphenyl ether (DPE) from Aldrich was used as-received. Methanol was used to extract the DPE from the polymer matrix.

2.2. Polymerization and polymer characterization

The polymerizations were carried out in a 1 L Büchi glass reactor under 2 bar of propene pressure and stirred at 1000 rpm. The Al (MAO)/Zr mole ratio was 1000. All reactions and manipulations were carried out in an inert gas atmosphere using standard Schlenk techniques. The polymerization reactions were stopped after 30 min and coagulated with excess HCl–acidified methanol, filtered, washed with methanol, water and acetone, and then dried. Polypropylene samples produced with Cat A were synthesized at 320 K (sPPA1) and 293 K (sPPA2), while those with Cat B were synthesized at 320 K (sPPB1) and 338 K (sPPB2).

Average molecular weights (M_w) and molecular weight distributions (M_w/M_n) were determined by gel permeation chromatography (GPC) on a Waters Alliance GPC2000 system equipped with a differential optical refractometer (model 150C). A set of three columns of type HT Styragel (HT3, HT4, and HT6) was used with 1,2,4-trichlorobenzene as solvent. The analyses were calibrated with narrow molecular mass distribution polystyrene and polyethylene standards. The flow rate was 1 mL/min at 408 K.

Tacticity and comonomer content were determined by ^{13}C nuclear magnetic resonance spectrometry (^{13}C NMR) recorded at 398 K on a Varian Inova 300 instrument operating at a Larmor frequency of 75 MHz. Solutions of the polymer samples were made in a mixture of *o*-dichlorobenzene and benzene-d_6 (20% v/v) and placed in 5 mm sample tubes.

The thermal properties were measured on a TA Instruments Modulated DSC 2920 differential scanning calorimeter (DSC) under a N_2 atmosphere to minimize thermal degradation. The experiment was started by heating each sample from 298 to 443 K at a rate of 40 K/min in order to eliminate any thermal history of the samples. To ensure complete melting, each sample was melted–annealed at 443 K for 5 min, and then cooled at 10 K/min to 233 K. The subsequent melting behavior was then observed by reheating the sample to 443 K at 10 K/min. The crystalline fraction (X_c) determinations were calculated from $X_c = \Delta H/\Delta H_o$, where ΔH is the measured melting enthalpy of a polymer, and ΔH_o, 196.6 J/g, is the enthalpy of fusion for a perfect crystal of sPP [25].

2.3. Phase diagrams

Glass capillary tubes containing varying ratios of polymer in diluent were sealed and heated in a Merck Model 9100 digital electrothermal melting point apparatus at 443 K for 5 min to ensure complete melting. The cloud points (the temperature at which turbidity first appears) were determined visually under optical lens eyeglasses incorporated into the equipment. Dynamic crystallization temperature of the sPP samples was measured by loading and sealing samples into capillary tubes as described above. Cooling was achieved by quenching the samples in liquid nitrogen, which yielded homogenous solid solutions that were used for thermal analysis on a TA Instruments Modulated DSC 2920 at a cooling rate of 10 K/min, and the onset of the exothermic peak during cooling was taken as the crystallization temperature [23].

2.4. Relative polymer–DPE solution viscosity

The relative viscosities of the polymer–DPE solutions were determined at 434 K using the falling ball method, which measures the time it takes for a spherical object to fall through a sample over a specific distance [23]. For this determination a 15 wt% polymer solution was used. A small, smooth, stainless steel sphere with a mass of 0.88 g and a diameter of 0.6 cm was dropped into the solution and the time required for it to fall between two marks measured. This measurement was repeated a minimum of five times to ensure repeatability, and the average value is reported.

2.5. Membrane preparation

Samples containing polymer–diluent mixtures (15 and 40 wt% of polymer) and an antioxidant (2,6-di-tert-butyl-4-methylphenol) were prepared in a test tube, which was purged under nitrogen and sealed to prevent oxidation. The test tubes were placed in an oven at 443 K for 48 h to homogenize the solution, and were then immediately cooled by immersion in a water bath at 298 K. Finally, the DPE in the membrane was extracted with methanol, and then dried.

2.6. Scanning electron microscopy observation

The resulting sPP microporous membranes were fractured in liquid nitrogen and coated with Au/Pd prior to observation using

Table 1
Main polymer properties.

Sample	M_w [Kg/mol]	M_w/M_n	Tacticity [%rr]	T_g [K]	T_c [K]	T_m [K]	X_c
sPPA1	90	1.6	89.6	273	353	393–405	0.23
sPPA2	160	1.7	96.5	274	396	416–422	0.31
sPPB1	300	1.8	88.3	276	341	392–402	0.19
sPPB2	180	1.7	84.5	274	326[a]	374–386	0.11

[a] Crystallization in the second heating scan associated with a cold crystallization process.

a LEO 1550 VP Gemini (ZEISS) scanning electron microscope to examine the morphology of membrane cross sections.

The average droplet size was determined by an image analyzer. The pore size of each sample was evaluated by measuring 40 and 20 random pores in the 40 wt% and 15 wt% polymer concentrations, respectively. Mean droplet diameter and standard deviation were used to evaluate pore size.

2.7. Matrix polymer crystal structure

The crystal structure that developed in the matrix of the porous membranes was evaluated using wide-angle X-ray diffraction (WXRD). Profiles of samples were obtained at room temperature on a Siemens D5000 diffractometer with $CuK_\alpha = 1.54$ Å and a step scan of 0.02°, between 2 and 30° 2θ.

3. Results and discussion

3.1. Polymer properties

Using the metallocene catalysts it was possible to synthesize a series of semicrystalline polymers in which one property, either tacticity or M_w, was changed by varying the catalyst or the polymerization conditions. The properties of these samples are reported in Table 1. Polypropylenes with higher syndiotacticity (sPPA1, SPPA2, and sPPB1) showed crystallization on cooling from the melt, and a double melting peak in the subsequent heating scan, which is associated with melt, recrystallization, and remelt processes. However, polymers with low syndiotacticity showed cold crystallization on heating, followed by a melting process (sPPB2); more details are given elsewhere[1] [26]. These properties strongly influence the final membrane morphology because polymer–solvent interactions, viscosity, and crystal behavior from polymer solution are important parameters when the membranes are prepared by the TIPS process.

3.2. Phase diagrams

The phase diagrams for sPPA1–DPE, sPPB1–DPE, sPPA2–DPE, and sPPB2–DPE polymer solutions are shown in Figs. 1 and 2. The trend lines were drawn by hand to guide the eye. These systems exhibited typical upper critical solution temperature (UCST) type phase behavior (cloud points) and dynamic crystallization temperatures. The monotectic point was located at ca. 50 wt% polymer concentration and it was possible to distinguish three different regions: one homogenous phase region (over the whole range of concentrations at a high enough temperature), and two phase regions, liquid–liquid (liquid–liquid demixing gap at polymer concentrations lower than 50 wt%) and solid–liquid (bellow the dynamic crystallization curve).

[1] Note: sPPA2y sPPB2 samples are referred to as sPPA3 and sPPB3, respectively, in Ref. [26].

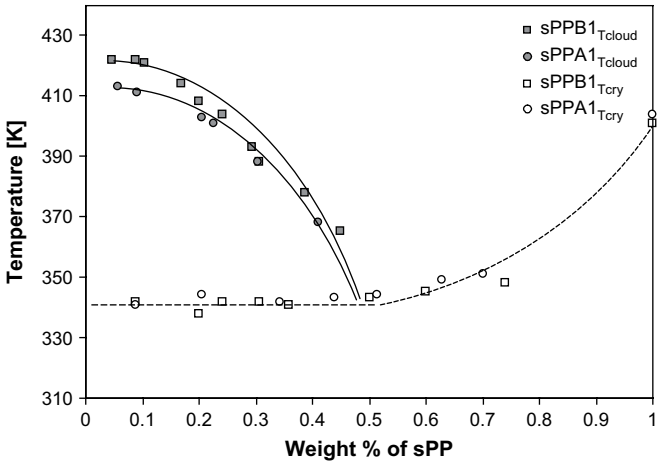

Fig. 1. Phase diagrams for sPPA1- and sPPB1–DPE systems: T_{cloud} represents the cloud points temperatures, T_{cry} represents the dynamic crystallization temperature.

As shown in Fig. 1, the cloud point curves of sPPA1 and sPPB1 were determined in order to evaluate the effect of the molecular weight of sPP. The UCST is shifted to higher values with increasing sPP molecular weight from 90 to 300 kg/mol in the low polymer concentration region (around 10 K). This change may be due to an entropy effect [14,27], the increase in M_w often enhances the entanglements between macromolecule chains and decreases the entropy contribution to the Gibbs free energy. The result is a shift in the cloud points curve toward higher temperature. On the other hand, the dynamic crystallization curve of these samples was located at the same temperatures depending only on their syndiotacticity.

In Fig. 2 it is possible to compare sPPA2 and sPPB2, which have similar M_w but different tacticities (96.5 and 84.5% rr, respectively). Their cloud point curves are located along the same master line as expected, without any influence of the differences in syndiotacticity [27]. But these systems exhibit a difference of around 30 K in their dynamic crystallization temperatures. These behaviors suggest that stereoregularity impacts crystallization behavior more than M_w in these polymer solutions.

Another observation comparing the crystallization temperature of the polymer (data are reported in Table 1) and the dynamic crystallization temperature of the polymer solution system (Figs. 1 and 2) was that the crystallization temperature of sPPA1 and sPPA2 is lower than that of the pure polymer (crystallization temperatures

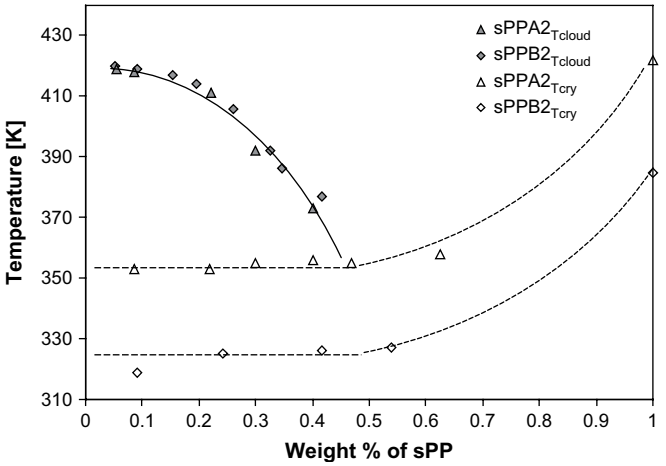

Fig. 2. Phase diagrams for sPPA2- and sPPB2–DPE systems: T_{cloud} represents the cloud points temperatures, T_{cry} represents the dynamic crystallization temperature.

Table 2
Relative viscosities of SPP–DPE solution at 15% polymer concentration.

Sample	Viscosity (g/cm s)
sPPA1	–
sPPA2	256
sPPB1	2432
sPPB2	60

decrease 10 and 43 K). The presence of the diluent increases the space for motion of the polymer chain and facilitates the generation of a crystal lattice [28]. However, the crystallization temperature of sPPB1 and sPPB2 samples was not affected by dilution. These samples have the highest molecular weights and lowest syndiotacticities, and it is likely that the effect of the diluent becomes negligible. However, further study is necessary in order to clarify this behaviour.

3.3. Relative polymer–DPE solution viscosities

Droplet growth kinetics in liquid–liquid phase separation of polymer–diluent systems is sensitive to the matrix phase viscosity. As the viscosity of the matrix phase increases, droplet growth rate decreases [13].

It is well known that sPP samples have zero shear viscosities approximately 10 times higher than iPP with the same M_w. In the solid state, sPP is a more expanded polymer because of the *trans* conformation of the backbone. It may be possible that the all *trans* conformation of sPP is not completely destroyed in the polymer melt, therefore a dominant *trans* conformation may continue to exist in the sPP melt [29].

In polymer solution, molecular weight, electrostatic repulsions, and steric hindrances contribute to increased viscosity. The viscosity data of 15 wt% sPP–DPE solutions are presented in Table 2. It was not possible to measure the viscosity of the sPPA1–DPE solution due to the limitations of the method (low viscosity of the solution). The influence of syndiotacticity and M_w was very significant; if we compare samples with similar syndiotacticity but different M_w (sPPA1 and sPPB1, Table 1) viscosity increased with M_w. On the other hand, in samples with similar molecular weight but different syndiotacticities (sPPA2 and sPPB2, Table 1), viscosity increased with stereoregularity, therefore it is not so easy to predict the viscosities of sPP solutions because they depend on both M_w and syndiotacticity. Similar behavior was observed in molten syndiotactic polypropylenes [30].

3.4. Membrane morphology

In many applications the interconnectivity of pores, pore size, and pore size distribution in porous membranes is very important. Since the final droplet size in the TIPS process is mainly dependent on the temperature difference between the cloud point and crystallization temperature [6], it is also necessary to take into consideration the quench depth (the difference between the cloud point and supercooling temperature). All the samples were quenched at 298 K in the solid–liquid region below their dynamic crystallization curve, which provides the driving force for phase separation as well as for polymer crystallization.

The SEM images of membrane cross sections of 40 wt% polymer solutions are presented in Fig. 3. The membranes show cellular pores, indicating that a liquid–liquid phase separation process took place. The sPPA2 membrane had the smallest cells, which were spherical and isolated. This membrane morphology is the result of small differences between could points and crystallization temperatures, which result in shorter growth time of the pores. The mean pore diameter was calculated at 4.2 μm, with a standard deviation of 0.6 μm.

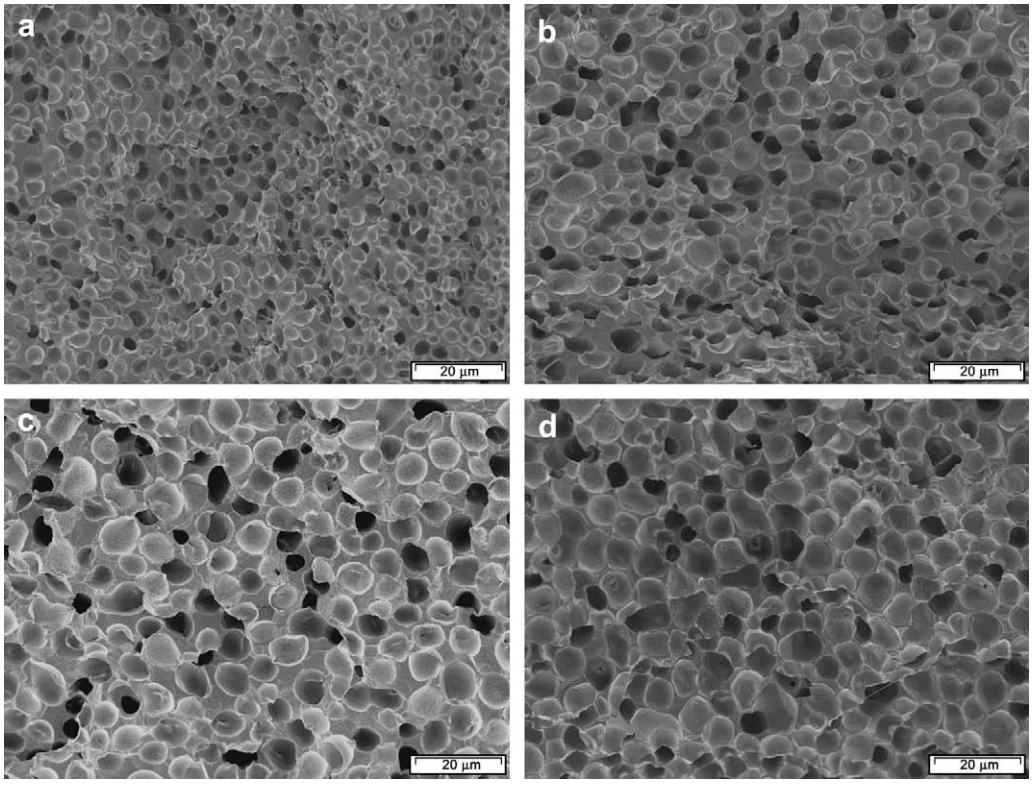

Fig. 3. Cross section membrane morphology of 40 wt% sample: (a) sPPA2, (b) sPPB2, (c) sPPA1 and (d) sPPB1.

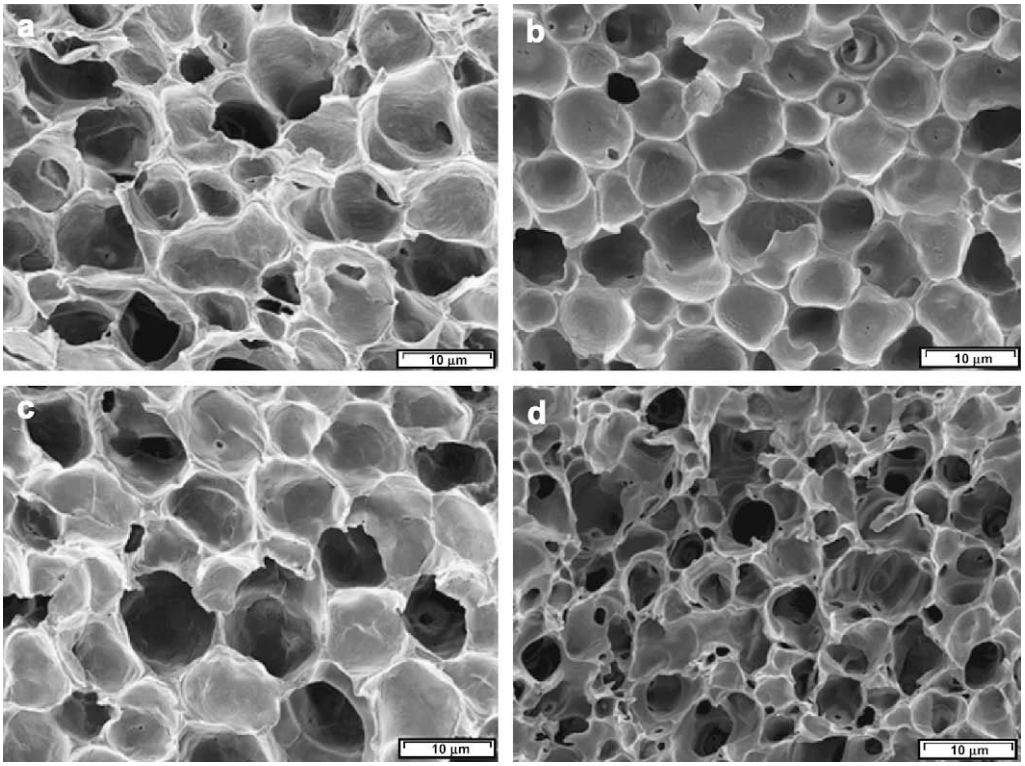

Fig. 4. Cross section membrane morphology of 15 wt% sample: (a) sPPA2, (b) sPPB2, (c) sPPA1 and (d) sPPB1.

The sPPA1 and sPPB1 membranes had larger pore sizes, with mean pore diameters of 7.3 and 7.6 μm, with standard deviations of 1 and 1.1 μm, respectively. The pores are less uniform spherical shapes and show pore interconnectivity caused by a longer growth period, (see below, greater difference between binodal and crystallization curve).

These morphologies of the samples were as expected according to the phase diagrams presented above. The distance between the cloud points curve and dynamic crystallization temperatures is appropriate for the liquid–liquid phase separation that occurred during cooling with less or no influence on polymer crystallization although all the samples quenched under crystallization, because the presence of diluent does not allow immediate crystallization, allowing enough time for liquid–liquid separation.

However, it was found that the sPPB2 sample had a somewhat larger pore size than sPPA2 (mean pore diameter of 5.8 μm and a standard deviation of 0.7 μm), but smaller than sPPA1 and sPPB1, contrary to what was expected, because the sPPB2 sample had the longest growth period and should therefore have the largest pore size. When a homogenous polymer–diluent solution is cooled, the droplets grow over time through a coarsening process. If the polymer crystallizes during liquid–liquid TIPS, droplet growth may be hindered or halted altogether. We assume that this is what happened with the sPPB2 samples, where there seems to be no further cell size increase, indicating that coarsening has been halted by early polymer crystallization [31].

Pore size is also dependent on kinetics aspects, and cooling rate, crystallization behavior, and droplet growth mechanism are important parameters in membrane morphology. Considering the latter aspect, droplet growth rate is strongly dependent on the viscosity of the polymer-rich phase and is approximately inversely proportional to it [13]. To further elucidate the influence of the polymer-rich phase viscosity; membranes from 15 wt% polymer solution were prepared. The cross sections of these membranes are shown in Fig. 4. According to these SEM images, pore size followed the order sPPB1 < sPPB2 < sPPA2 < sPPA1. Even though sPPB1 and sPPA1 samples present the same crystallization temperature in the phase diagrams, the viscosity of sPPA1 is lower, allowing faster droplet growth and yielding larger pore sizes (mean pore diameter of 8.9 μm and a standard deviation of 1.5 μm). As shown in Fig. 4, sPPB1 had the smallest pore size and highest interconnectivity, which is in agreement with a high polymer solution viscosity retarding the coalescence process.

Although sPPA2 had the shortest growth period, it presents higher viscosity than sPPA1, causing these two samples to have similar pore size. The sPPB2 sample presents the same behavior observed at 40% (no further pore size increase because it was stopped by early polymer crystallization).

These results show that viscosity is not an essential parameter in the final membrane morphology of 40 wt% polymer concentration. However, in contrast to the 40% solution, it was found to be an important factor at lower concentrations.

While the cloud point and crystallization temperature differences serve in many respects to predict pore size, it was found that other factors also had a critical role. Therefore, knowing the microstructure of sPP and polymer solution concentration, microporous membranes having controlled pore size can be produced.

Finally, the membranes prepared from the sPPA2 sample should have the smallest pore size and fewer interconnection, but it is possible to use them at high temperatures due to their higher melting point. On the other hand, although membranes made from polymers sPPA1 and sPPB1 should have similar pore sizes, good interconnectivity, and similar operating temperature range, sPPB1 presents the advantage of having a higher molecular weight that makes it more manageable.

3.5. Matrix polymer crystal structure

In general, syndiotactic polypropylene exhibits polymorphic structures, which depend on crystallization conditions and the

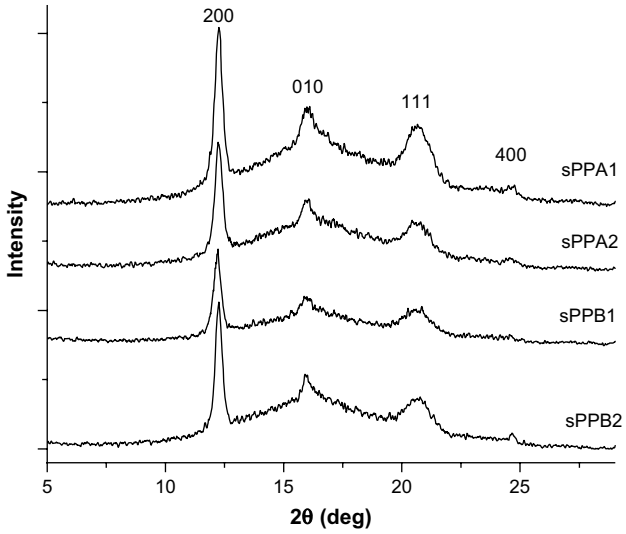

Fig. 5. Membrane X-ray diffraction patterns.

stereoregularity of the sample [20]. In order to see the crystal structure of the syndiotactic polypropylenes in the membranes which were obtained after the TIPS process, samples produced using a 15 wt% polymer solution were examined by WXRD, Fig. 5. The samples presented the same patterns, indicating that they have the same crystal structures after rapid crystallization from solution. The crystal phase present is the most stable and common disordered Form I, characterized by chains in the $s(2/1)$ helical conformation packed in orthorhombic unit cells having axes $a = 14.5$ Å, $b = 5.6$ Å, $c = 7.4$ Å. This occurrence of this possible disorder may be related to the statistical substitution of right- and left- handed helices about each axis (a and b) of the unit cell, giving rise to a statistical departure from regular fully antichiral packing along both axes [32–34]. This structure is characterized by the presence of 200 and 010 reflections at $2\theta = 12.2^\circ$ and 15.9°, respectively, and the absence of the 211 reflection at $2\theta = 18.8^\circ$ in the X-ray diffraction patterns.

4. Conclusions

The sPP–DPE systems had typical liquid–liquid phase separation with a monotectic point at about 50 wt% polymer concentration. The cloud points were slightly affected by molecular weight and the effect more prominent at low polymer concentration. The dynamic crystallization curve temperatures were mainly dependent on the polymer's syndiotacticity, regardless of its molecular weight. These two thermodynamic polymer solution properties determined the droplet growth period.

The final membrane morphology depends on the droplet growth period, but when the samples were quenched bellow the crystallization temperature, the liquid–liquid phase separation could be halted by early polymer crystallization when the growth period is very deep; therefore no further cell size increase occurred.

At lower polymer concentrations, pore size also depends strongly on the viscosity of the polymer-rich liquid matrix phase, but at higher polymer concentrations the effect of viscosity was negligible.

The microporous membranes showed similar X-ray profiles indicating that each of the sPP samples developed the same crystal structure after the TIPS process.

Acknowledgments

The authors acknowledge the financial support of CONICYT (FONDAP Project 11980002), and the Deutscher Akademischer Austauschdienst (DAAD) for a Ph.D. scholarship to María Eulalia Vanegas. The helpful collaboration of Dr. Wilfredo Yave is especially acknowledged. Further the authors extend their thanks to K. Prause (GKSS) for SEM analysis.

References

[1] Ulbricht M. Polymer 2006;57:2217–62.
[2] Kools WFC Winchester, European Patent Office EP1362633A1; 2003.
[3] Castro AJ. United States Patent 4247498; 1981.
[4] Lloyd D, Kinzer K, Tseng HS. J Membr Sci 1990;52:239–61.
[5] Cui ZY, Xu YY, Zhu LP, Wang JY, Zhu BK. Ionic 2008, doi:10.1007/s11581-008-0253-9.
[6] Kim LU, Kim CK. J Polym Sci Part B Polym Phys 2006;44:2025–34.
[7] http://www.membrana.com/research/development.htm [accessed October 2008].
[8] Jeon MY, Kim CK. J Membr Sci 2007;300:172–81.
[9] Kosaraju PB, Sirkar KK. J Membr Sci 2008;321:155–61.
[10] Van de Witte P, Dijkstra PJ, Van den Berg JW, Feijen J. J Membr Sci 1996; 117:1–31.
[11] Laxminarayan A, Mc Guire K, Kim S, Lloyd D. Polymer 1994;35:3060–9.
[12] Mc Guire K, Lloyd D, Lim G. J Membr Sci 1993;79:27–34.
[13] Mc Guire K, Laxminarayan A, Martula D, Lloyd D. J Colloid Interface Sci 1996;182:46–58.
[14] Matsuyama H, Maki T, Teramoto M, Asano K. J Membr Sci 2002;204:323–8.
[15] Matsuyama H, Teramoto M, Kudari S, Kitamura Y. J Appl Polym Sci 2001;82: 169–77.
[16] Matzuyama H, Okafuji H, Maki T, Teramoto M, Tsujioka N. J Appl Sci 2002;84: 1701–8.
[17] Yave W, Quijada R, Serafín D, Lloyd D. J Membr Sci 2005;263:146–53.
[18] Yave W, Quijada R, Lloyd D, Cerrada ML, Benavente R, Ulbricht M. Macromol Mater Eng 2006;291:155–61.
[19] Chen G, Lin Y, Wang X. J Appl Polym Sci 2007;105:2000–7.
[20] De la Rosa C, Auriemma F. Prog Polym Sci 2008;31:145–237.
[21] Rojo E, Fernandez M, Muñoz ME, Santamaría A. Polymer 2006;47:7853–8.
[22] Sakata Y, Unwin AP, Ward IM. J Mater Sci 1995;30:5841–9.
[23] Yave W, Quijada R, Serafín D, Lloyd D. J Membr Sci 2005;263:154–9.
[24] Yave W, Quijada R, Ulbricht M, Benavente R. Polymer 2005;46:11582–90.
[25] Haftka S, Konnecke K. J Macromol Sci Phys 1991;B30:319–34.
[26] Vanegas ME, Quijada R, Serafini D, Galland G, Palza H. J Polym Sci Part B Polym Phys 2008;46:798–806.
[27] Lee H, Myerson A, Levon K. Macromolecules 1992;25:4002–10.
[28] Tao H, Zhang J, Wang X, Gao J. J Polym Sci Part B Polym Phys 2007;45:153–61.
[29] Eckstein A, Friedrich C, Lobbrecht A, Spitz R, Mülhaupt R. Acta Polym 1997;48:41–6.
[30] Rojo E, Muñoz ME, Santamaría A, Peña B. Macromol Rapid Commun 2004;25: 1314–8.
[31] Cho I, Kim J, Kim S. Korea Polym J 1997;5:191–8.
[32] Lotz B, Lovinger A, Cais R. Macromolecules 1988;21:2375–82.
[33] De Rosa C, Auriemma F, Vinti V. Macromolecules 1997;30:4137–46.
[34] Sevegney M, Kankan R, Siedle A, Naik R, Naik V. Vib Spectrosc 2006;40: 246–56.